JACS
JOURNAL OF THE AMERICAN CHEMICAL SOCIETY
Article
pubs.acs.org/JACS

Iron Complex-Catalyzed Ammonia–Borane Dehydrogenation. A Potential Route toward B–N-Containing Polymer Motifs Using Earth-Abundant Metal Catalysts

R. Tom Baker,*[,†] John C. Gordon,*[,‡] Charles W. Hamilton,[‡,∥] Neil J. Henson,[§] Po-Heng Lin,[†] Steven Maguire,[†] Muralee Murugesu,[†] Brian L. Scott,[⊥] and Nathan C. Smythe[‡]

[†]Department of Chemistry and Centre for Catalysis Research and Innovation, University of Ottawa, Ottawa, Ontario Canada K1N 6N5

[‡]Chemistry Division, [§]Theoretical Division, and [⊥]Materials Physics and Applications Division, Los Alamos National Laboratory, Los Alamos, New Mexico 87545, United States

Supporting Information

ABSTRACT: Ammonia–borane (NH_3BH_3, AB) has garnered interest as a hydrogen storage material due to its high weight percent hydrogen content and ease of H_2 release relative to metal hydrides. As a consequence of dehydrogenation, B–N-containing oligomeric/polymeric materials are formed. The ability to control this process and dictate the identity of the generated polymer opens up the possibility of the targeted synthesis of new materials. While precious metals have been used in this regard, the ability to construct such materials using earth-abundant metals such as Fe presents a more economical approach. Four Fe complexes containing amido and phosphine supporting ligands were synthesized, and their reactivity with AB was examined. Three-coordinate $Fe(PCy_3)[N(SiMe_3)_2]_2$ (**1**) and four-coordinate $Fe(DEPE)[N(SiMe_3)_2]_2$ (**2**) yield a mixture of $(NH_2BH_2)_n$ and $(NHBH)_n$ products with up to 1.7 equiv of H_2 released per AB but cannot be recycled (DEPE = 1,2-bis(diethylphosphino)ethane). In contrast, Fe supported by a bidentate P–N ligand (**4**) can be used in a second cycle to afford a similar product mixture. Intriguingly, the symmetric analogue of **4** (Fe(N–N)(P–P), **3**), only generates $(NH_2BH_2)_n$ and does so in minutes at room temperature. This marked difference in reactivity may be the result of the chemistry of Fe(II) vs Fe(0).

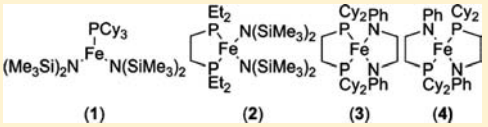

INTRODUCTION

Hydrogen (H_2) has been proposed as an alternative power source, both as a transportation fuel and, through its use in a PEM fuel cell, as a replacement for batteries for portable electricity.[1] In the former case, the U.S. Department of Energy (DOE) has set performance targets such that a vehicle could travel approximately 300 miles on a single charge.[2,3]

The details of the full spectrum of approaches funded by the DOE have been covered elsewhere,[4−14] but one approach investigated within the DOE Chemical Hydrogen Storage Center of Excellence is the use of ammonia–borane (NH_3BH_3, AB) as a hydrogen carrier. AB contains 6.5, 13.1, and 19.6 wt % H_2 for the loss of the first, second, and third equivalents of H_2, respectively. As in all chemical storage approaches, however, the ultimate utility of AB depends upon finding ways to efficiently remove[15,16] and replace H_2.[17] With an arena as large as the transportation sector, this also requires materials that are both cheap and abundant.

Another important application related to dehydrogenation of amine–boranes is the development of new BN-containing polymeric materials. For example, $(H_2NBH_2)_n$ can be thought of as an inorganic analogue of polyethylene and $(HNBH)_n$ as an inorganic analogue of polyacetylene. While cyclic compounds such as $(HNBH)_3$ (borazine, a benzene analogue) and $(H_2NBH_2)_3$ (cyclotriborazane, CTB, a cyclohexane analogue) as well as the *n*-butane analogue $H_3NBH_2NH_2BH_3$[18] are well characterized, the identity and controlled synthesis of higher order oligomers and polymers is more nebulous.[19] This is in stark contrast to the mature field of polyolefin chemistry, where the emphasis is on fine-tuning control over parameters such as tacticity and polydispersity. Manners and co-workers have recently demonstrated the utility of employing metal-catalyzed dehydrocoupling for the synthesis of B–N and B–P materials from amine– and phosphine–boranes,[20−22] and this area would also benefit by the development of efficient earth-abundant metal catalysts.

Metal-based catalysts offer the potential to tune *both rate and extent* of hydrogen (H_2) release from AB. Systems employing transition metals have provided both the fastest rates (in the case of Ir,[23] Ru,[24,25] and Pd[26]) and the largest extent of H_2 loss (in the case of Ni[27] and Ru[15,16]) yet reported for AB dehydrogenation under reasonable reaction conditions. Further tunability has been reported through the use of ionic liquids as the reaction medium.[28] Unfortunately, many of these systems use relatively expensive metals (Rh,[29] Ir, Ru, and Pd) or suffer from catalyst instability under the reaction conditions (Ni, Pd). We have recently investigated the synthesis, characterization, and modes of reactivity of Fe-based catalysts, as these have the potential to be much more cost-effective toward scale-up on a

Received: November 17, 2011
Published: March 19, 2012

 © 2012 American Chemical Society dx.doi.org/10.1021/ja210542r | J. Am. Chem. Soc. 2012, 134, 5598−5609

global scale. $FeH(CH_2PMe_2)(PMe_3)_3$[30] has been shown to exhibit mild reactivity at 20 °C, while Manners et al. recently reported the formation of borazine and B-(cyclodiborazanyl)-aminoborohydride (BCDB) from the photolytic activation of $[CpFe(CO)_2]_2$.[31] We describe herein some of our recent results toward developing efficient Fe-based AB dehydrogenation catalysts and their potential utility for aminoborane polymer synthesis.

Bifunctional Catalysis for Ammonia–Borane Dehydrogenation. Developing effective catalysts for AB dehydrogenation requires control over two fundamental reaction pathways (Scheme 1). The initial dehydrogenation of AB and

Scheme 1. Divergent Reaction Pathways Lead to Different AB Dehydrogenation Products[32]

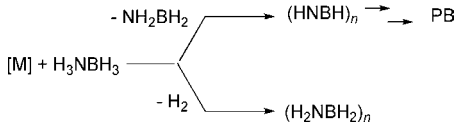

the release of 1 equiv of H_2 forms aminoborane (H_2NBH_2) which is unstable and reacts with further AB in two reported ways depending on the nature of the catalyst employed.[32] In some cases, such as the aforementioned Ir catalyst, exclusive formation of insoluble $(H_2NBH_2)_n$ corresponds to rapid release of a single equivalent of H_2 per molecule of AB at room temperature (lower pathway, Scheme 1).[21,23] Several catalysts, based on Rh and Ni, as well as Williams's bifunctional Ru catalyst, however, afford greater than 2 equiv of H_2 per molecule of AB.[16,27,29] The Ni-based catalyst is reported to yield almost exclusively cross-linked borazine, i.e. polyborazylene (PB), and greater than 2.5 equiv of H_2 per molecule of AB. These reactions are typically slower than those with the Ir- and other Ru-based[15,16,24,25] catalysts and require heating and/or longer reaction times. Attempts to further dehydrogenate the colorless, insoluble, $(H_2NBH_2)_n$ product were unsuccessful under reasonable conditions with any of the above catalysts, confirming that divergent reaction pathways are in operation.

While the intimate details of the different mechanisms of dehydro-oligomerization are not yet fully understood, a key step that differentiates between these pathways was recently identified via the use of an aminoborane trapping agent, cyclohexene.[32,33] Trapping of aminoborane in the form of Cy_2BNH_2 (Cy = cyclohexyl) occurs predominantly in catalyzed reactions exhibiting greater extents of H_2 release, suggesting that efficient release of aminoborane from the metal center (presumably forming a hydrogen or dihydride complex; upper pathway, Scheme 1), affords borazine and PB, while complexes that bind aminoborane form singly dehydrogenated $(H_2NBH_2)_n$ (lower pathway, Scheme 1). Consistent with this hypothesis, use of the Ir catalyst at higher temperatures afforded some borazine and PB presumably due to some dissociation of aminoborane from the metal center. Moreover, computational studies[34−36] indicated that the key BN-ethylcyclobutane intermediate, BCDB, results from intermolecular oligomerization of aminoborane via the novel $H_2NBHNH_2BH_3$ intermediate, accounting for the significant rate decrease on dilution.[37]

These observations point to the importance of bifunctional catalysts[38−40] in metal-catalyzed AB dehydrogenation as aminoborane is precluded from binding to the metal (Scheme 2). While initial bifunctional systems afforded active Ru catalysts,[24,25] predominant formation of insoluble $(BH_2NH_2)_n$ suggests that

Scheme 2. AB Dehydrogenation Using a Bifunctional Catalyst

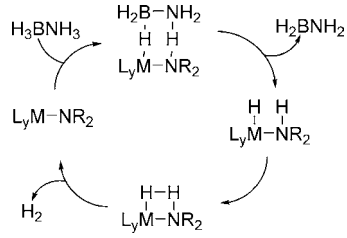

other reaction pathways are operating. In contrast, recent work by Williams et al.[16] has identified an efficient bifunctional Ru catalyst that affords exclusively borazine and PB at 80 °C. We now report the preparation and characterization of amido iron phosphine complexes and their evaluation as potential bifunctional catalysts for AB dehydrogenation.

RESULTS

Generation of Amido Iron Complexes and Preliminary Reactivity with Ammonia–Borane. As might be expected, treatment of $Fe[N(SiMe_3)_2]_2$ (**A**)[41] with a THF solution of AB resulted in immediate formation of a dark precipitate, presumably containing iron metal. Addition of PCy_3 to **A** as a stabilizing agent yielded crude material (later shown to contain **1**, Scheme 3) that was capable of generating greater than 1 equiv of H_2 per AB, but the reaction required heating which again led to formation of black precipitate during the course of the reaction. In an attempt to improve this stability further, we employed a chelating phosphine in the form of 1,2-bis(diethylphosphino)ethane (DEPE) (**2**, Scheme 3). In this case, there was again significant AB dehydrogenation at 60 °C, and darkening of the reaction solution was accompanied by formation of the bis(borane) adduct of DEPE and the protonated amido ligand $NH(SiMe_3)_2$, likely a poor ligand for iron. This deficiency was addressed by treatment of **A** with *N*,*N*′-diphenyl-1,2-ethylenediamine $[(PhHNCH_2)_2]$, which afforded a blue paramagnetic material (**B**). While **B** and excess AB exhibited initial gas evolution, formation of a black precipitate limited conversion to less than two turnovers. Reaction of **B** with 1,2-bis(dicyclohexylphosphino)ethane (DCPE), gave a red complex, later identified as **3** (Scheme 3). Complex **3** exhibited rapid dehydrogenation of AB at room temperature, but was not able to be recycled with a second batch of AB due to decomposition through ligand loss (*vide infra*). In order to protect against ligand (phosphine) loss from **3**, its asymmetrically bridged cousin was developed (**4**, Scheme 3). While **4** is more robust than **1**, its reactivity is markedly different despite the structural similarities (*vide infra*).

Synthesis of Complexes 1−4. X-ray crystallographic data for compounds **1**−**4** are summarized in Table 1.

Complex 1. The most straightforward synthesis of **1** was accomplished by addition of $FeCl_2$ to a THF solution of PCy_3 (presumably forming $FeCl_2(PCy_3)$ *in situ*, which has some solubility in THF). Subsequent addition of $KN(SiMe_3)_2$ resulted in darkening of the reaction mixture. The pentane-soluble components of this mixture yielded a dark solution from which **1** could be crystallized. The use of other solvents, other iron halides, or shorter times between PCy_3 and base addition generally resulted in lower yields or no product formation (with a concomitant increase in the formation of black precipitate). When isolated cleanly (a process that generally

dx.doi.org/10.1021/ja210542r | J. Am. Chem. Soc. 2012, 134, 5598−5609

Scheme 3. Optimized Syntheses of Complexes 1−4 and Their AB Dehydrogenation Selectivity

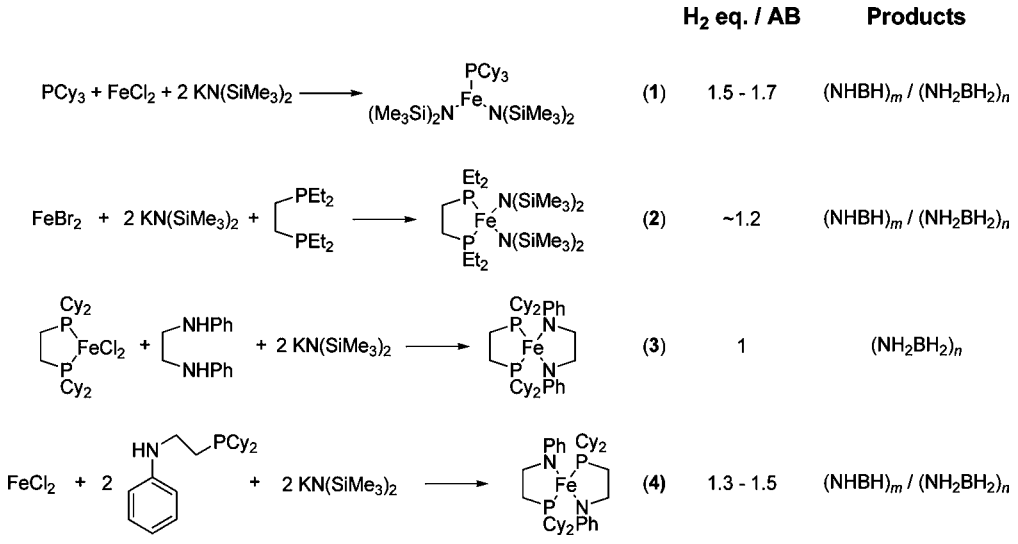

Table 1. X-ray Crystallographic Structural Parameters for Complexes 1−4

	1[42]	2[42]	3	4
formula	$C_{30}H_{69}FeN_2PSi_4$	$C_{22}H_{60}FeN_2P_2Si_4$	$C_{44}H_{70}FeN_2OP_2$	$C_{40}H_{62}FeN_2P_2$
fw (g/mol)	657.05	582.87	760.81	688.71
T (K)	120(1)	200(2)	120(1)	140(1)
crystal system	monoclinic	tetragonal	monoclinic	monoclinic
space group	$P2_1/n$	$P4_1$	$P2_1/c$	$P2_1/n$
a (Å)	12.0279(9)	11.9184(3)	11.677(3)	11.443(13)
b (Å)	15.7960(12)	11.9184(3)	22.210(5)	20.06(2)
c (Å)	20.3153(16)	24.2844(8)	16.123(4)	16.304(19)
α (°)	90	90	90	90
β (°)	90.3290(10)	90	100.869(3)	99.697(19)
γ (°)	90	90	90	90
V (Å^3)	3859.7(5)	3449.56(17)	4106.4(16)	3690(7)
Z	4	4	4	4
GoF	1.124	1.042	1.089	0.941
R [$I > 2\sigma(I)$] (%)	R_1 = 3.9	R_1 = 2.9	R_1 = 7.8	R_1 = 7.3
	wR_2 = 8.8	wR_2 = 5.9	wR_2 = 18.1	wR_2 = 12.8
R (all data) (%)	R_1 = 6.1	R_1 = 3.7	R_1 = 16.9	R_1 = 22.1
	wR_2 = 9.6	wR_2 = 6.1	wR_2 = 22.0	wR_2 = 18.4

requires 3−4 crystallizations from cold pentane), **1** is essentially colorless with only a very slight greenish-blue hue. While it is unclear if this slight coloring is the result of a small amount of impurity or an inherent property of the molecule, we tend to favor the former explanation as multiple crystallizations decrease the intensity of the color. **1** is highly air-sensitive and will scavenge trace oxygen to form an orange solid. The relatively low isolated yield of **1** is a result of its high solubility in pentane and the need for multiple crystallization steps.

The molecular structure of **1**[42] (Figure 1) determined by single-crystal X-ray diffraction reveals a 3-coordinate Fe center with close to trigonal planar geometry. This is shown by the N(2)−N(1)−P(1)−Fe(1) dihedral angle of ca. 1.6°, which puts Fe at 0.03 Å out of the N(1)−N(2)−P(1) plane. At 128.46(7)°, the N(1)−Fe(1)−N(2) angle is slightly greater than 120°, creating a small distortion as seen by the N(1)−Fe(1)−P(1) and N(2)−Fe(1)−P(1) angles of 115.16(5)° and 116.31(5)°, respectively. The Fe−N bonds are 1.9496(16) and

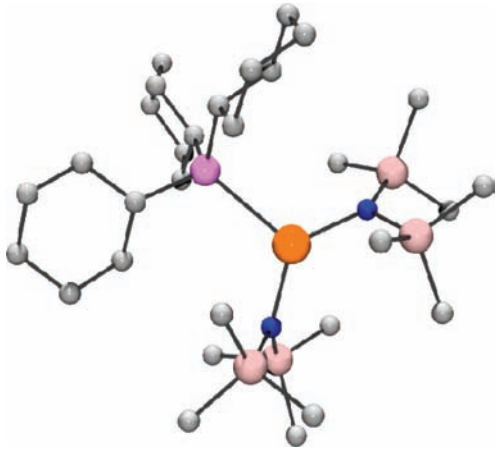

Figure 1. Ball-and-stick representation of the crystallographically determined molecular structure of **1**.[42] Fe (orange), N (blue), Si (pink), and P (orchid) with hydrogen atoms omitted.

dx.doi.org/10.1021/ja210542r | J. Am. Chem. Soc. 2012, 134, 5598−5609

1.9503(16) Å for Fe−N(1) and Fe−N(2), and the Fe−P bond is 2.5167(6) Å. Complex **1** is paramagnetic, with a χT of 5.16 cm^3·K/mol (300 K), indicating that it is high spin, although this is much larger than the expected spin-only value. Our explanation for the source of this behavior is reported elsewhere.[42]

Complex ***2***. **2** was synthesized by *in situ* formation of $Fe[N(SiMe_3)_2]_2$ from $FeBr_2$ and $KN(SiMe_3)_2$. The brownish solid that was collected after subsequent addition of DEPE was extracted with hexanes and crystallized to give the complex illustrated in Figure 2.[42] The Fe−N(1) and Fe−N(2) bond

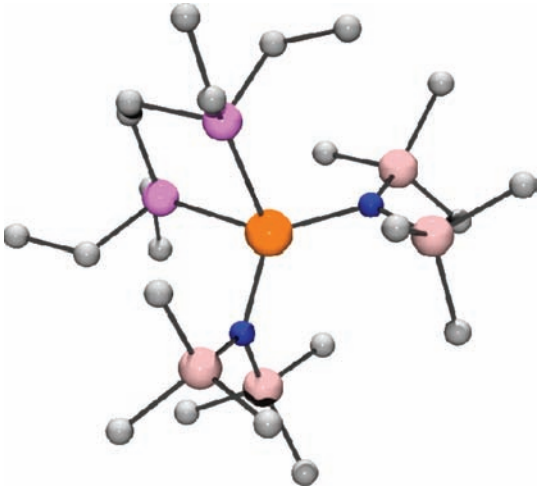

Figure 2. Ball-and-stick representation of the crystallographically determined molecular structure of **2**.[42] Fe (orange), N (blue), Si (pink), and P (orchid) with hydrogen atoms omitted.

lengths of 1.9949(15) and 1.9886(15) Å are slightly longer than the corresponding bonds in **1**, as are the Fe−P(1) and Fe−P(2) lengths of 2.5965(5) and 2.5878(5) Å. The bond angles result in a distorted tetrahedron with the P(1)−Fe−P(2) angle (78.454(17)°) significantly less than the N(1)−Fe−N(2) angle (120.93(6)°). Compared to **1**, N(1)−Fe−N(2) is slightly more acute. Significant twisting of the tetrahedron is shown by the angle pairs of N(1)−Fe−P(1) and N(2)−Fe−P(2) (129.06(5)° and 126.22(5)°) compared to N(1)−Fe−P(2) and N(2)−Fe−P(1) (99.24(5)° and 98.33(5)°). **2** is high spin with a χT value (300 K) of 3.20 cm^3·K/mol.

Complex ***3***. The direct synthesis of **3** was accomplished by addition of $[(PhHNCH_2)_2]$ to a solution of $FeCl_2$(DCPE) in toluene or THF to form a yellow solution, followed by deprotonation with $KN(SiMe_3)_2$. The resultant red solution yielded an air-sensitive, dark red crystalline product upon isolation by addition of pentane and collection of the resulting precipitate. While **3** is quite soluble in toluene and ethereal solvents, it exhibits limited solubility in aliphatic solvents. **3** is paramagnetic with a χT value (300 K) of 2.71 cm^3·K/mol, close to the spin-only value for a high-spin, tetrahedral d^6 ion. The molecular structure (Figure 3) reveals it to be a pseudo-tetrahedral complex with an average N(x)−Fe−P(x) angle of ca. 121.3°, but N(1)−Fe−N(2) and P(1)−Fe−P(2) angles of 91.13(18)° and 84.30(6)°, respectively. The Fe−N(1) and Fe−N(2) bond lengths are 1.923(4) and 1.938(5) Å, while the Fe−P(1) and Fe−P(2) bond lengths are 2.4015(17) and 2.3974(17) Å.

Complex ***4***. The synthetic route to the HNP ligand required for the synthesis of **4** is summarized in Scheme 4. While direct

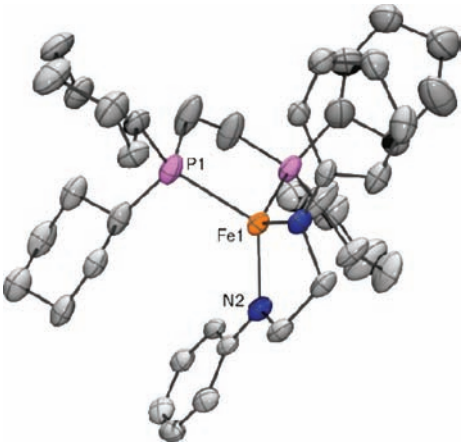

Figure 3. Crystallographically determined molecular structure of **3**. Hydrogen atoms and solvent are omitted for clarity, and thermal ellipsoids are shown at 50% probability level.

Scheme 4. Preparation of the HNP Ligand Used in the Synthesis of 4

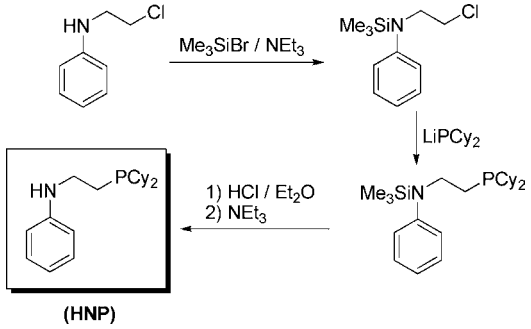

reaction of *N*-(2-chloroethyl)-benzenamine with $LiPCy_2$ in THF yielded HNP on a small scale, larger scale reactions showed significant byproduct formation as a result of the unprotected N−H bond. Attempts at protecting this position using Me_3SiCl were unsuccessful as the reaction did not go to completion; however, substitution with Me_3SiBr in this step gave essentially quantitative conversion. The HNP ligand is a colorless solid that is soluble in common organic solvents. A 2 equiv portion of HNP was used to solubilize $FeCl_2$ in THF, followed by deprotonation with $KN(SiMe_3)_2$. The resulting product could be isolated as an air-sensitive orange solid (**4**) from toluene. Complex **4** is paramagnetic with a χT of 3.88 cm^3·K/mol (300 K) significantly larger than **3**, despite the gross similarity of the ligand environments (Figure 4). The Fe−N(1) and Fe−N(2) bond lengths are 1.959(5) and 1.961(6) Å, and the corresponding Fe−P bonds are 2.422(3) and 2.423(3) Å. These are slightly longer than what is seen in **3**. The internal N(1)−Fe−P(1) and N(2)−Fe−P(2) angles of 85.85(18)° and 84.02(18)° are closest to the P−Fe−P angle in **3**. Of the other angles in the pseudotetrahedron, the N(2)−Fe−N(1) angle at 136.1(2)° stands out as significantly different than the N(2)−Fe−P(1), N(1)−Fe−P(2), and P(1)−Fe−P(2) angles of 119.95(17)°, 117.53(17)°, and 116.55(10)°. This represents a spread among the external angles (difference between the largest and smallest) of 19.6° vs 1.6° in **3**.

Reactivity of Complexes 1−4 with AB. Addition of AB to a THF or diglyme solution of complex **1** resulted in an immediate darkening and some gas release. However, AB was

dx.doi.org/10.1021/ja210542r | *J. Am. Chem. Soc.* 2012, 134, 5598−5609

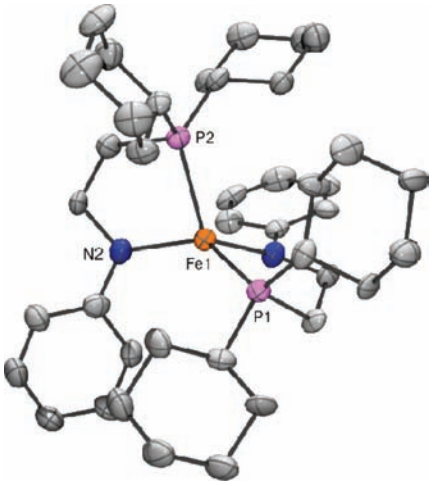

Figure 4. Crystallographically determined molecular structure of **4** with hydrogen atoms omitted for clarity. Thermal ellipsoids are shown at 50% probability level.

not completely consumed unless heat (60 °C) was applied, and additional PCy_3 was added. Without additional PCy_3, the active species decomposed into a black precipitate before all the AB was consumed. In this regard, by adding 0, 1, or 2 equiv or an excess (i.e., 1 equiv per mole of AB) of PCy_3, it was observed that an additional 2 equiv of PCy_3 per Fe center (3 total P/Fe) was the optimal amount; 1 equiv did not prevent decomposition, and excess PCy_3 yielded a greater quantity of the corresponding phosphine–borane. It is readily apparent from the ^{11}B NMR data that higher order dehydrogenation products (i.e., polyborazylene) were formed (Scheme 3 and Figure 5).

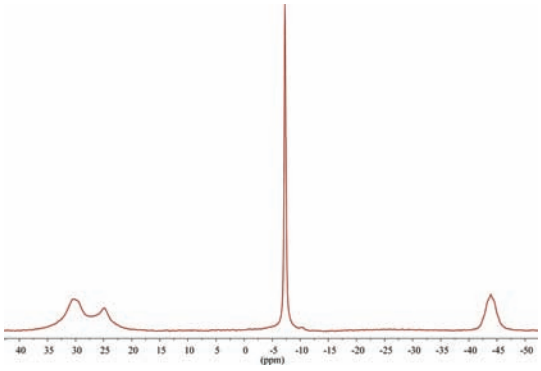

Figure 5. ^{11}B NMR spectrum (baseline corrected) of the dehydrogenation of AB using **1** plus 2 equiv of PCy_3 at 60 °C with added $NaBPh_4$ as an internal standard shows PB (ca. 20–35 ppm), $NaBPh_4$ (−7.29 ppm), and PCy_3BH_3 (ca. −44 ppm).

Gas buret measurements carried out at 60 °C indicate that up to 1.7 equiv of H_2 were released over a period of hours (Figure S8) which is consistent with calibrated (internal $NaBPh_4$) ^{11}B NMR spectral data, suggesting that ca. 30–50% insoluble PAB is also formed in this reaction.

AB dehydrogenation results using 5 mol % **2** were similar to those of **1** in terms of both rate and the array of dehydrogenation products formed. After 4 h at 60 °C the ^{11}B NMR spectrum shows a typical mixture of soluble dehydrogenation products (Figure 6). At 60 °C, the reaction is complete in 20 h with formation of PB, PAB, and phosphine–borane (Figure S9). Decomposition of complex **2** is evidenced by formation of

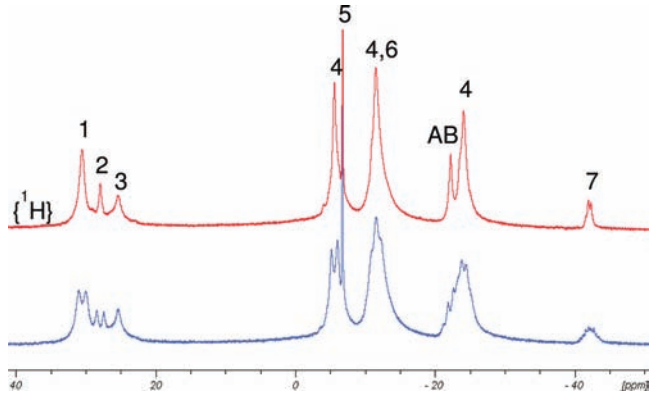

Figure 6. ^{11}B NMR spectra of AB dehydrogenation using 5 mol % **2** at 60 °C for 4 h with added $NaBPh_4$ (**5**) as an internal standard (^1H decoupled spectrum on top. Products include borazine (**1**), PB (**3**), BDCB (**4**), CTB (**6**), and phosphine–borane (**7**). The resonance assigned as **2** and shoulder on resonance assigned to **4** may be due to $H_2NBHNH_2BH_3$.[35]

$HN(SiMe_3)_2$, significant darkening of the solution, and formation of uncharacterized diamagnetic Fe phosphine complexes (Figure S10).

The addition of ca. 20 equiv of AB to a THF or diglyme solution of **3** resulted in an immediate darkening in color. After a short induction period (ca. 2 min, concentration dependent), rapid effervescence was observed. By ^{11}B NMR spectroscopy, the AB was completely consumed in 15 min. If the concentration of **1** was lowered to 2 mol %, complete consumption of AB was observed after 2 h. An insoluble white precipitate formed during the course of these reactions, and filtration of the reaction mixture after completion gives a solution that does not contain any boron containing species (beyond trace materials in the baseline) by ^{11}B NMR spectroscopy (Figure 7).

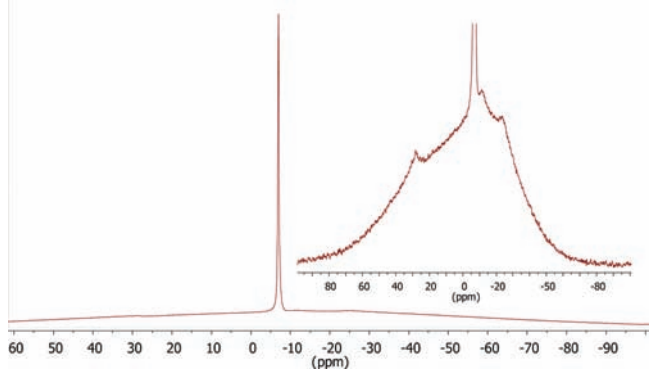

Figure 7. ^{11}B NMR spectrum of AB dehydrogenation using **3**. This shows (added) $NaBPh_4$ as essentially the only soluble boron-containing species remaining after AB consumption.

This indicates selective generation of poly(aminoborane) (PAB), which was confirmed by increasing the scale of the reaction and isolation of the off-white precipitate. Based on consistency with the FTIR spectroscopic data (Figure S7) of $[NH_2BH_2]_n$ obtained from IrH_2(POCOP) by Goldberg et al. and recently elucidated by Manners et al.,[21] this product is assigned as PAB. **3** decomposes during the course of polymerization as can be seen by the appearance of multiple ^{31}P NMR peaks (Figure 8), a suspected hydride peak in the ^1H NMR at ca. −18 ppm, and that the reaction mixture is unreactive to further AB addition.

dx.doi.org/10.1021/ja210542r | J. Am. Chem. Soc. 2012, 134, 5598–5609

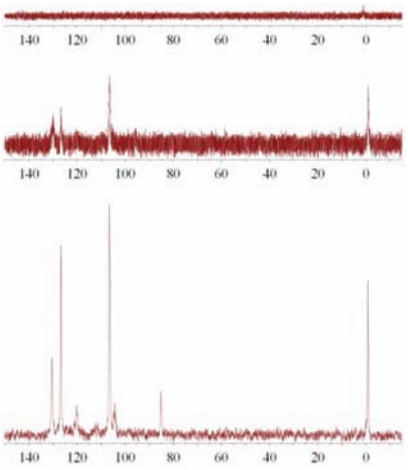

Figure 8. ^{31}P NMR spectra of **3** + AB in THF showing the decomposition of **3** over time: 0 min (top), 10 min (middle), and ca. 20 h (bottom).

Addition of AB (20 equiv) to a diglyme or THF solution of **4** at room temperature causes a darkening of the solution and shows a mixture of AB along with singly and doubly dehydrogenated products (approximately 0.8 equiv of H_2 total with minimal phosphine–borane formation) after ca. 20 h. Increasing the temperature to 60 °C gives a mixture of insoluble PAB and soluble PB and singly dehydrogenated products along with unreacted AB and phosphine–borane after ca. 3 h. Increasing the reaction time to 20 h allowed for the complete consumption of AB, with only PB and phosphine–borane present in solution (Figure S12). The amount of H_2 produced was ca. 1.3 equiv. While some decomposition was observed per the formation of black precipitate over the course of dehydrogenation and evidenced by the presence of phosphine–borane, the catalytically active species remained active for a second cycle. When an additional 20 equiv of AB was added and the reaction mixture was heated to 60 °C, the AB ^{11}B NMR signal disappeared after 24 h with a concomitant increase in the quantity of PB (ca. 1.5 equiv of H_2, 46% PB, Figure S13). This is in contrast to **3** where reactivity is lost after the first cycle, and **1** where complete decomposition to bulk iron is eventually observed. Thus, despite its structural similarity to **3**, the reactivity of **4** with AB is more akin to that of **1** and **2**. Some possible reasons for this are discussed in the next section.

DISCUSSION

a. Selectivity Differences in Iron Complex-Catalyzed AB Dehydrogenation. *Considerations for Initiation and Propagation.* Compared to the Ru complexes described by Fagnou et al.[24] and Schneider et al.,[25] the PNNP-Fe transfer hydrogenation catalysts described by Morris et al.,[43−47] and the PNNP-Ir complexes described by Gao et al.,[48,49] **1**–**4** are much more sterically hindered as shown by their space-filling models (Figure 9) and supported by initial DFT calculations carried out on **1** that showed that there was no viable approach for AB without the ligand sphere around **1** relaxing in some manner. Thus, any explanation for the reactivity of these molecules with AB requires accounting for this fact.

The AB dehydrogenation activity of the potentially bifunctional Ru complexes reported by Fagnou and Schneider were proposed to proceed in a manner analogous to that of Noyori transfer hydrogenation (i.e., bifunctional activation of AB, Scheme 2). DFT calculations reported by Fagnou et al.

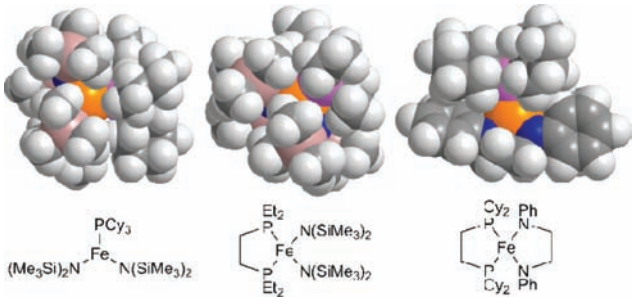

Figure 9. Space-filling models of **1** (left), **2** (middle), and **3** (right).

supported this interpretation, and Schneider reported kinetic isotope effects that were consistent with bifunctional activation. Nonetheless, formation of insoluble polyaminoborane suggests that *initially formed aminoborane remains bound to the metal*, and Schneider even reported such a complex in which the boron is coordinated to the amido nitrogen atom (Figure 10).[50,51] In

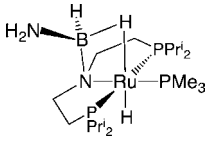

Figure 10. Structure of Ru–N-coordinated aminoborane reported by Schneider et al.[50]

short, a necessary implication of the formation of PAB is that the *NH_2BH_2 remains bound to the metal center during propagation.* Similar conclusions have recently been reached in a comprehensive mechanistic study of dimethylamine–borane dehydrogenation catalyzed by bis(phosphine) Rh cations.[52]

b. Possible Reaction Pathways for 1 and 2. The reactivity of **1** toward AB is indicative of a precatalyst that eventually undergoes decomposition. We believe that darkening of color upon AB addition to **1** is the result of its reduction to a phosphine-solubilized Fe(0) species (*vide infra*) and loss of the poor ligand $HN(SiMe_3)_2$. The importance of the presence of PCy_3 is illustrated by the effect of adding additional phosphine to the reaction between **1** and ca. 20 equiv of AB. At 60 °C and after long reaction time (overnight) to ensure the reaction is over, unreacted AB remains in solution. Adding 1 equiv of PCy_3 (relative to **1**) decreases the amount of residual AB, while addition of 2 equiv (relative to **1**) of PCy_3 results in complete consumption (Figure 5). However, addition of excess of PCy_3 (1:1 AB:PCy_3) decreased PB yield and increased the quantity of PCy_3BH_3 by 1.5–2 times that of the case when 2 equiv of PCy_3 per Fe center are used while decreasing the formation of black precipitate. The implication of this is that the excess phosphine is stabilizing the catalytically active species.

Upon sitting for weeks, the stoichiometric reaction between **1** and AB at room temperature yielded dark crystals for which an X-ray structure indicates an Fe_9 cluster (Figure 11). While the data suffered from significant disorder and attempts to resynthesize the material for a more detailed analysis were unsuccessful, we believe that this structure provides some insight into what is happening upon AB addition. The cluster itself consists of nine Fe(0) atoms arranged as alternating triangles capped at the ends with PCy_3 molecules. There is insufficient room for any more than six PCy_3 ligands, and although the X-ray data cannot rule out the presence of hydrides, their presence has not been observed upon AB addition to **1** by ^1H NMR.

dx.doi.org/10.1021/ja210542r | J. Am. Chem. Soc. 2012, 134, 5598–5609

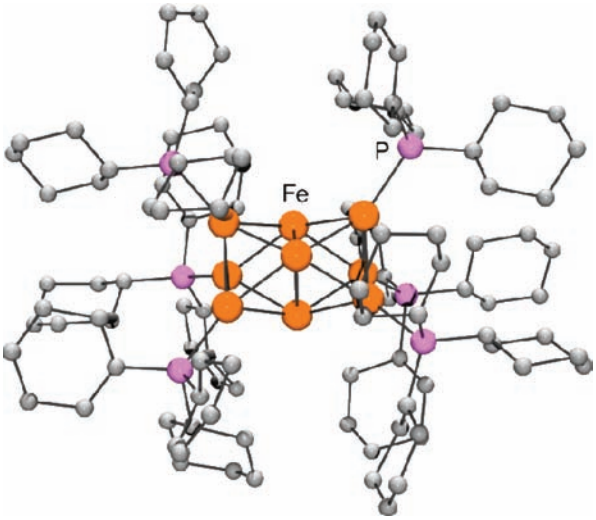

Figure 11. Connectivity of the Fe_9 cluster.

Identification of this $Fe_9(PCy_3)_6$ cluster compound lends some credence to the proposal that the first step in the reaction of **1** with AB is reduction of divalent iron and the formation of soluble Fe(0) species. The dehydrogenation activity observed is not just due to bulk Fe(0) since a commercial sample of iron powder exhibited negligible activity with or without the presence of PCy_3. In order to investigate the reduction mechanism further, simple quantum chemical calculations were carried out using density functional theory. Calculations were performed on models of **1** and **2** with both Fe(II) and Fe(0) centers using the Gaussian09 software (Revision B.01)[53] involving full geometry optimization at the PBE-h level[54] with the LANL08 basis set on iron (LANL2DZ+5s5p2d+f),[55] and a 6-31+G* basis set for the ligand orbitals. A LANL2DZ effective core potential was used for iron. Models were constructed using the crystallographically derived structural data elucidated in the earlier section, and the Fe(0) complexes were treated as the dianions. Although it is not being suggested that the Fe(0) models represent actual intermediate structures in the reduction pathway to the Fe_9 cluster, the calculations do provide an indication of the type of electronic and structural changes taking place as a consequence of the two-electron reduction process. The first finding from the calculations is that the high-spin model is predicted to be the most stable for both **1** and **2**, by 295.4 and 265.3 kJ mol^{-1}, respectively. A summary of the structural parameters for the minimized structures is given in Table 2. The calculated bond lengths also show closer agreement to experiment for the high-spin models. The plausibility of the proposed reduction mechanism is further supported by the predicted decrease in Fe−P bond length on going from the calculated optimized structures between Fe(II) and Fe(0) models. This concept of the active catalyst being a solubilized Fe(0) aggregate is also consistent with the observation that addition of excess PCy_3 minimizes the formation of black precipitate. Due to the similarities in the product distribution between **1** and **2** and their initial ligand environments, it is likely that they follow similar reaction pathway(s).

c. Reaction Pathways of 3 and 4. Complex **3** is unique in both the increased AB dehydrogenation reaction rate (competent at 25 °C) and its selectivity in forming PAB. It also differs from **1** and **2** in that the parent amine of its amido ligand $(PhHNCH_2)_2$, as demonstrated by **B**, *vide supra*) is a much stronger ligand than $HN(SiMe_3)_2$. The induction period observed upon AB addition to a solution of **3** would also be consistent with the latter's role as a precatalyst. The active species formed from **3** decomposes during the course of dehydrogenation (Figure 8), presumably at least partially into iron metal based on the formation of black precipitate. This decomposition is also reflected by the lack of observed dehydrogenation when a second 20 equiv of AB are added. While this makes it impossible to attempt to isolate the active form of **3**, ^{31}P NMR data indicate that loss of the chelating phosphine is occurring, while ^{11}B NMR shows that this does not result in formation of phosphine−borane.[56] Thus it is possible that reaction of **3** with AB is preceded by dissociation of one of the chelating phosphine arms. The activity of **3** toward AB is consistent with the divergent pathway proposal of Baker et al. (*vide supra*) as addition of excess cyclohexene to the reaction mixture does not lead to any trapping of NH_2BH_2 (Figure S6).

Table 2. Calculated and Experimental Bond Lengths for Compounds 1 and 2 Showing the Effect of Spin State and Change in Oxidation State of the Iron Center (Spin States: Fe(II) low spin, Singlet; Fe(II) High Spin, Quintet; Fe(0) High Spin, Triplet)

		Fe−P (Å)	Fe−N (Å)
compound **1**	experiment	2.62	1.93
	Fe(II), high spin	2.58	1.95
	Fe(II), low spin	2.32	1.85
	Fe(0) high spin	2.32	2.10
compound **2**	experiment	2.60	1.99
	Fe(II), high spin	2.63	1.98
	Fe(II), low spin	2.26	1.99
	Fe(0), high spin	2.33	2.05

In an attempt to shed additional light upon the operation of catalyst **3**, we investigated its reactivity with 10 equiv of dimethylamine−borane (DMAB). After 12 h at 20 °C, most of the DMAB was converted into a mixture of the cyclic dimethylaminoborane dimer, the diaminoborane $HB(NMe_2)_2$, and the linear product $NHMe_2BH_2NMe_2BH_3$ (Figure S14). Close inspection of the resulting ^{11}B NMR spectra, however, also revealed formation of the diazaborane compound **5**, which

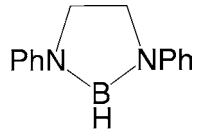

5

was obtained independently from reaction of $(NHPhCH_2)_2$ with borane−THF (Figures S15, S16). This then points to an additional catalyst decomposition pathway, namely borane complexation to the basic amido- or amine arm of the N−N chelate, similar to the situation observed by Schneider et al.[50] discussed above. In any case, it is clear that the ultimate fate of **3** is decomposition and loss of activity, as it cannot be used to dehydrogenate a second batch of AB. The unsymmetrical **NP** ligand was therefore utilized in order to isolate a more robust version of **3** with similar steric and electronic properties such that if phosphine dissociation occurred in **4**, one atom per ligand would still remain bound to the iron center, as compared to complete dissociation of the chelating phosphine in **3**. Surprisingly, **4** behaves more similarly to **1** and **2** with respect

dx.doi.org/10.1021/ja210542r | J. Am. Chem. Soc. 2012, 134, 5598−5609

to AB dehydrogenation. The following section attempts to address why this is the case.

d. Formation of Poly(aminoborane): Some Mechanistic Observations. Due to the selective and rapid formation of PAB with **3**, this complex intrigued us as a possible route to the controlled polymerization of B−N materials if catalyst robustness issues could be addressed. A first step for PAB formation is likely via coordination of the BH_3 moiety, either via bridging hydrides or through a σ-type B−H bond interaction. These are well-established binding motifs within metal complexes containing Rh, Ir, and Ru.[57−64] In the case of an Ir complex, Weller et al. have observed coordination of a BH_3 unit to Ir, with no evidence for formation of a terminal metal hydride containing the H−Ir−BH_2 unit (Figure 12).[64] This group also

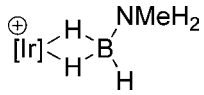

Figure 12. $NMeH_2BH_3$ binding to an Ir complex.[64]

demonstrated the dimerization of BH_3NH_2Me, however the proposed mechanism in this case cannot account for higher order linear oligomers as it depends upon proximity of the terminal NH group to the metal center in order to release H_2 and form the dimer (Scheme 5).

Scheme 5. Dimerization of BH_3NMeH_2 As Proposed by Weller and Co-Workers[64]

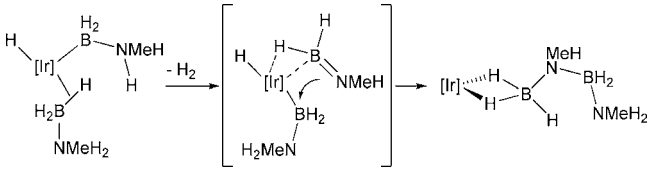

*Complex **3**: Pathway A.* The induction period in the reaction of 3 with AB may signify the reversible dissociation of one arm of the phosphine chelate followed by ligation of AB via the Lewis basic B−H bond to give **C** (Scheme 6). Protonation of the amido nitrogen would then afford the amidoborane complex **D** followed by dissociation of the amino arm, allowing room for ligation of a second equivalent of AB to give **E**. Subsequent rapid dehydrogenative insertion steps could then build the polymer chain in an analogous fashion to that of Ziegler−Natta polymerization of olefins. While amidoborane complexes like **D** have only been isolated for electrophilic metals such as Mg, Ca, and Zr,[65] β-H elimination to give Fe-coordinated η^2-H_2BNH_2 intermediates (**F**), as characterized for Ru by Sabo-Etienne et al. and Rh by Weller et al., could also be an important step in the chain propagation.

*Complex **3**: Pathway B.* Alternatively, coordination of the NH_2BH_2 fragment to Fe via the BH_2 group of aminoborane (e.g., **F**) could also result in end-chain propagation (Scheme 7). Such a species could also be accessed if, after loss of coordination of one of the phosphine arms, AB could coordinate in a manner similar to that observed in the Rh, Ir, and Ru systems (Figure 12). If an Fe−H moiety is formed (Scheme 8, pathway i) and the chelating amide is protonated, the result would also be a bound NH_2BH_2 unit. Alternatively, the coordinated AB could dehydrogenate directly (Scheme 8, pathway ii), which has been observed with BH_3NMe_2H and Ir.[63] While ^{1}H NMR indicates the presence of Fe−H at the end of catalysis, decomposition renders this inconclusive.

Interestingly, Fagnou's calculations on a Ru-NP′ complex (NP′ = $NH_2CH_2CH_2PMe_2$) also point to the feasibility of end-chain propagation and proton transfer from substrate to ligand (Figure 13, complex **H**).[24] While there are insufficient data to draw any definitive conclusions with respect to the role of species such as **G**, **H**, and **I** in this particular case, end-chain propagation would also explain the formation of PAB. On the other hand, our previous report of selectivity control of AB dehydrogenation in ionic liquids,[28] in which better coordinating anions discouraged formation of PAB, is more consistent with a coordination polymerization mechanism.[51]

*Complex **4**: Comparisons with Complex **3**.* Both of the mechanisms shown in Schemes 6 and 8i illustrate pathways by which **4** could be more susceptible than **3** toward ligand loss (Scheme 9). Our original motivation for synthesizing the mixed NP donor ligand was to prevent ligand loss by tethering the bulky P-donor atom to an amide group, rather than to another phosphorus atom. However, a side effect of this is that the acute N−Fe−P angle draws the tethered N- and P-substituents closer together while simultaneously increasing N(1)−P(2) and N(2)−P(1) (i.e., trans atom) distances.

If proton transfer upon AB binding is indeed a mechanistic step, the closest proton-acceptor atom in proximity to the ligated AB moiety is the amide nitrogen contained within the now monodentate NP ligand (i.e., **J** in Scheme 9). It is expected that the $(Me_3Si)_2N^-$ ligands within **1** and **2** are readily prone to protonation and subsequent dissociation, leading to metal-based reduction (based on the observed precipitate formation). Thus, it appears to be the case that complex **4** also undergoes ligand dissociation and metal-based reduction in an analogous fashion to **1** and **2**. In contrast, however, in the case of complex **3**, chain initiation and propagation to form PAB is faster than competing protonation/ligand dissociation chemistry which eventually leads to catalyst decomposition. Additionally, phosphine−borane is not observed in the polymerization of AB by **3** due to the lower temperature employed compared to **1**, **2**, and **4**.

CONCLUSIONS

While AB possesses attractive properties for use as a transportation-based H_2 fuel carrier, its thermal decomposition characteristics are unsuitable for practical deployment. Thus, the catalyzed dehydrogenation of AB is a promising methodology to circumvent this, although care must also be taken that any "spent fuel" form is also amenable to regeneration under realistic conditions.[17] Due to the scale of the transportation sector, any catalyst must also be comprised of elements that are globally abundant. To this end, we have explored the use of Fe-based complexes as catalytically active templates for AB dehydrogenation.

Herein we have demonstrated AB dehydrogenation using four Fe-based complexes supported by mixed amido/phosphine ligands. While the identity of the catalytically active species is unclear in each case, it is likely that complexes **1**−**4** are in fact precatalysts that react with AB to form the active catalytic species. The nature of precatalyst activation and its subsequent effect on coordination and dehydrogenation of AB appears to be a key factor in understanding the marked reactivity differences between **3** (increased rate) and **1**, **2**, and **4** (increased extent). Another influence is whether or not reduction of Fe(II) to soluble Fe(0) species is required in order to form higher order dehydrogenation products. Furthermore, the

dx.doi.org/10.1021/ja210542r | J. Am. Chem. Soc. 2012, 134, 5598−5609

Scheme 6. Possible Initiation Mechanism for the Reaction of 3 with AB, Dictating the Formation of PAB

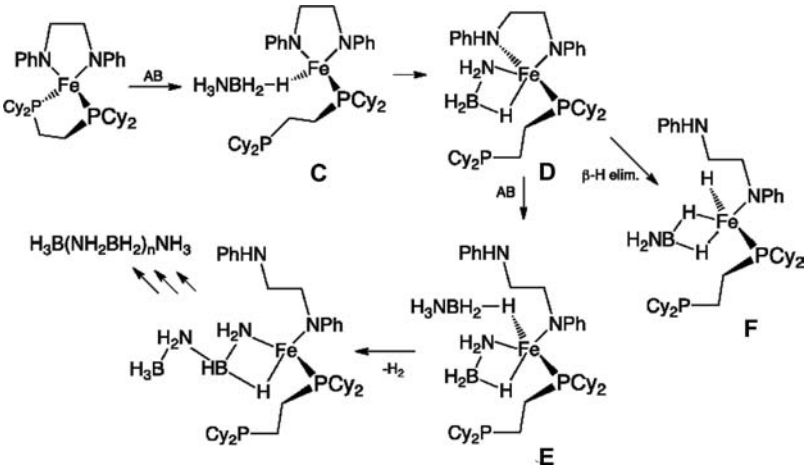

Scheme 7. End-Chain Propagation of AB Polymerization by 3

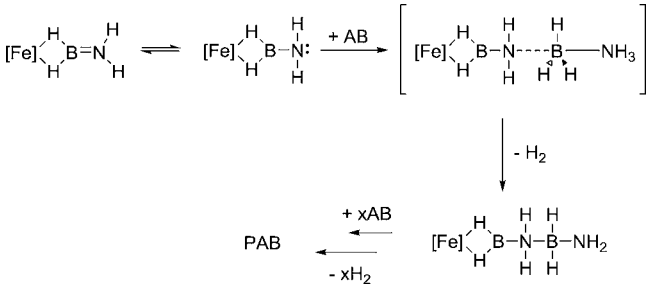

observed reactivity of **3** may point toward the synthesis of chemically robust Fe complexes that exhibit rapid, selective polymerization of amine–boranes. Our observation of B–N bond formation with the N–N ligand in complex **3** also points to the need to control the basicity at N in bifunctional catalysts for this application if they are to compete with those developed by Williams et al. that employ a Lewis *acidic* main group center that is to date only effective with Ru. Such general designed catalytic approaches to selective formation of PB are particularly important if robust, supported catalysts are to be developed for practical use with hydrogen fuel cells.

EXPERIMENTAL SECTION

All manipulations involving air-sensitive compounds were performed in an Ar-filled glovebox or using standard Schlenk techniques.

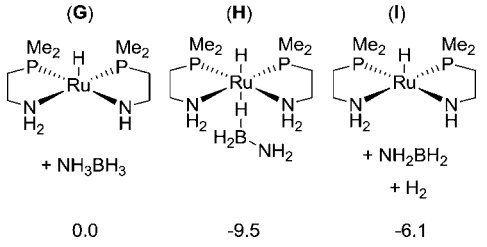

Figure 13. Selected calculated intermediates during the dehydrogenation of AB by Ru-NP′ as reported by Fagnou et al.[24] ΔG(298 K) energies in THF (**F** is lowest energy conformer) are in kcal/mol.

Scheme 9. Possible Pathway for Enhanced Ligand Loss from 4

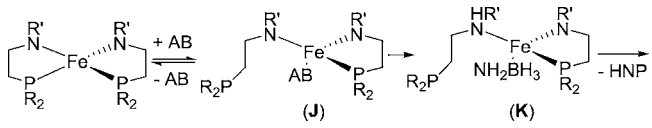

Anhydrous solvents were obtained from Aldrich or Acros and stored over 4 Å molecular sieves under an Ar atmosphere in a glovebox. NEt_3 (Aldrich) was stored over 4 Å molecular sieves. Chemicals dimethylamine–borane, borane-THF, *N,N′*-diphenylethylenediamine, $KN(SiMe_3)_2$, *n*BuLi, Me_3SiBr, HCl/Et_2O, C_2Cl_6, Fe powder, *N*-(2-hydroxyethyl)aniline and $NaBPh_4$ (Aldrich), DCPE, $FeCl_2$, PCy_3, $HPCy_2$, and PPh_3 (Strem) were purchased commercially and used as received. Complexes **1** and **2** were synthesized as previously reported.[42] NMR spectra were obtained on a Bruker AV400 spectrometer and

Scheme 8. Possible Initiation Steps Involving Boron-Bound AB in the Case of 3: Pathway (i) Invokes Fe–H Formation; Pathway (ii) Invokes Direct Dehydrogenation

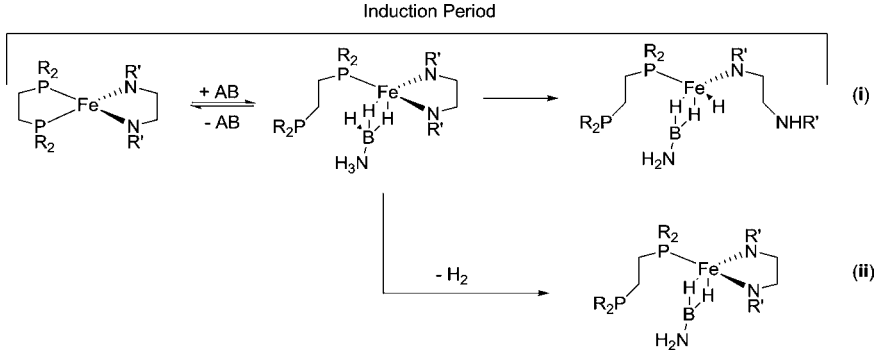

dx.doi.org/10.1021/ja210542r | J. Am. Chem. Soc. 2012, 134, 5598–5609

referenced to 85% H_3PO_4 in H_2O (^{31}P, 0 ppm) or $NaBPh_4$ (^{11}B, −7.29 ppm). Elemental analyses were performed by Atlantic Microlab (Norcross, GA). The magnetic susceptibility measurements were obtained using a Quantum Design SQUID magnetometer MPMS-XL7 operating between 1.8 and 300 K for dc-applied fields ranging from −7 to 7 T. Dc analyses were performed on polycrystalline samples of 10.2 and 20.0 mg for **3** and **4**, respectively, packed in grease and capsule under a field ranging from 0 to 7 T between 1.8 and 300 K. Crystals of **3** and **4** were mounted in a nylon cryoloop from Paratone-N oil under argon gas flow. The data were collected on a Bruker D8 diffractometer, with APEX II charge-coupled-device (CCD) detector, and Bruker Kryoflex low-temperature device. The instrument was equipped with graphite monochromatized Mo Kα X-ray source (λ = 0.71073 Å), and a 0.5 mm monocapillary. A hemisphere of data was collected using ω scans, with 10-s frame exposures and 0.5° frame widths. Data collection and initial indexing and cell refinement were handled using APEX II[66] software. Frame integration, including Lorentz-polarization corrections, and final cell parameter calculations were carried out using SAINT+[67] software. The data were corrected for absorption using redundant reflections and the SADABS[68] program. Decay of reflection intensity was not observed as monitored via analysis of redundant frames. The structure was solved using direct methods and difference Fourier techniques. All hydrogen atom positions were idealized and rode on the atom they were attached to. The final refinement included anisotropic temperature factors on all non-hydrogen atoms. For **3**, two disordered carbon atoms in a cyclohexyl ring were each modeled in two one-half occupancy positions, and hydrogen atom positions were not included for the disordered atoms. Structure solution, refinement, and creation of publication materials were performed using SHELXTL.[69] ORTEP diagrams were created using ORTEP-3.[70] The extent of H_2 release from AB was measured either through use of a gas buret or by integration of the ^{11}B NMR spectrum against the internal $NaBPh_4$ standard. In the latter case, PB/borazine products were treated as generating 2 equiv of H_2 and PAB (inferred from unaccounted for ^{11}B in the product spectrum) was treated as having released 1 equiv of H_2. In cases of phosphine−borane formation, the phosphine−borane is counted as producing 0 equiv of H_2.

Synthesis of 3. $FeCl_2$(DCPE) (1.40 g, 2.55 mmol) was added to a 20 mL scintillation vial, to which was added toluene (ca. 15 mL). *N*,*N*′-Diphenylethylenediamine (541 mg, 2.55 mmol) was subsequently added to give a brown mixture that was allowed to stir for ca. 1 h. Upon addition of $KN(SiMe_3)_2$ (1.02 g, 5.11 mmol), the mixture turned red. The mixture was filtered through Celite to give a red solution that was then concentrated and cooled to ca. −25 °C. The resulting solid was collected and dried *in vacuo* (580 mg, 33%). Anal. $C_{40}H_{62}FeN_2P_2$ (calcd) C: 68.50 (69.76), H: 8.89 (9.07), N: 3.98 (4.07). χT at 300 K = 2.71 cm^3·K/mol (μ_{eff} = 4.66 μ_B).

Synthesis of 4. The HNP ligand (1.00 g, 3.15 mmol) and $FeCl_2$ (200 mg, 1.58 mmol) were added to a 20 mL vial followed by THF (ca. 15 mL). After the $FeCl_2$ was all dissolved, $KN(SiMe_3)_2$ (628 mg, 3.15 mmol) was added to yield a dark red mixture. The mixture was filtered through Celite and washed with THF (3 × 15 mL) to give a red solution. This solution was reduced to dryness, and the residue was taken up in toluene and filtered again. The resulting filtrate was concentrated, and two crops were collected of an orange solid (729 mg, 67%).

Anal. $C_{40}H_{62}FeN_2P_2$ (calcd) C: 69.61 (69.76), H: 8.94 (9.07), N: 4.15 (4.07). χT at 300*K* = 3.88 cm^3·K/mol (μ_{eff} = 5.57 μ_B).

Synthesis of *N*-(2-Chloroethyl)benzenamine. This compound has been reported in the literature.[71] Alternatively, *N*-(2-hydroxyethyl)aniline (10.3 g, 75.1 mmol) was added to a 300 mL round-bottom flask followed by CH_2Cl_2 (ca. 80 mL). The resulting solution was cooled in an ice bath before addition of C_2Cl_6 (19.6 g, 82.8 mmol). To this, PPh_3 (21.7 g, 82.7 mmol) was slowly added in portions using a powder funnel. After complete addition of PPh_3, the funnel was washed with CH_2Cl_2 (ca. 20 mL). The reaction was subsequently left to warm to room temperature overnight. The resulting white precipitate was collected, added to H_2O (ca. 150 mL), and quenched with 3 equiv of $NaHCO_3$. The product was extracted with CH_2Cl_2 (3 × 100 mL) and dried with Na_2SO_4. After solvent removal on a rotary evaporator, the very pale yellow oil was degassed and further dried over 4 Å molecular sieves before storage at ca. −25 °C (7.8 g, 67%). ^1H NMR (benzene-d_6): δ 2.88 (m, 2H), 3.04 (t, 2H), 3.37 (bs, 1H), 6.29 (m, 2H), 6.73 (tt, 1H), 7.09 (m, 2H).

Synthesis of HNP. *N*-(2-Chloroethyl)benzenamine (6.00 g, 38.6 mmol) was added to a Schlenk flask followed by CH_2Cl_2 (ca. 20 mL) and NEt_3 (8.1 mL, 58.1 mmol). The reaction mixture was cooled in an ice bath, and Me_3SiBr (5.6 mL, 42.4 mmol) was added dropwise using an addition funnel. The reaction was then allowed to warm to room temperature overnight. The solvent was removed *in vacuo*, and the resulting residue was taken up in pentane and filtered through Celite. Removal of pentane yielded the protected aniline as a cloudy colorless oil (7.5 g, 85%). ^1H NMR (benzene-d_6): δ 0.09 (s, 9H), 3.14 (t, 2H), 3.34 (t, 2H), 6.80−6.90 (m, 3H), 7.09 (m, 2H).

$HPCy_2$ (1.00 g, 5.04 mmol) was added to a 20 mL vial followed by THF (ca. 10 mL), and the resulting solution was cooled to ca. −25 °C. Cold *n*BuLi (2.5 M in hexanes, 2.02 mL, 5.05 mmol) was added via syringe in 3 portions with cooling of the reaction mixture back down to ca. −25 °C in between additions. The resulting yellow mixture of $LiPCy_2$ was cooled to ca. −25 °C. In a separate vial, the protected aniline (1.15 g, 5.05 mmol) in THF (ca. 2 mL) was also cooled. Once cooled, the protected aniline was added dropwise to the $LiPCy_2$ mixture to give an orange solution. After stirring for ca. 2 h, the volatiles were removed *in vacuo*, and the residue was taken up in Et_2O and filtered. Excess HCl/Et_2O (2 M) was added to the filtrate resulting in the formation of white precipitate. The mixture was stirred overnight. The white solid was subsequently collected, washed with Et_2O (2 × 10 mL), added to a THF/NEt_3 mixture (ca. 7 mL/10 mL), and left stirring for 5 days. After filtration through Celite, volatiles were removed from the filtrate *in vacuo* to give a colorless solid (1.17 g, 60%) that was used without further purification (see Figures S18, S19 for ^1H and ^{31}P NMR spectra). ^1H NMR (benzene-d_6): δ 1.00−1.90 (m, 24H), 3.17 (m, 2H), 3.60 (bs, 1H), 6.56 (d, 2H), 6.76 (t, 1H), 7.19 (t, 2H). $^{31}P\{^1H\}$ NMR (benzene-d_6): δ −10.16 (s).

Dehydrogenation of AB. In a typical dehydrogenation experiment, AB and $NaBPh_4$ were added to a 4 mL vial followed by ca. 1.5−2 mL of diglyme. Once the solids dissolved, the metal complex was added to the solution, and the vial was *loosely* capped to allow for the escape of H_2. For experiments that required heating, the vial was placed in a heating block. At the end of the run, the sample was filtered through Celite into a 5 mm NMR tube. Typical quantities used: **3**, 8.2 mg, 0.012 mmol; AB, 7.3 mg, 0.237 mmol; and $NaBPh_4$, 27.7 mg, 0.081 mmol.

Bulk Dehydrogenation of AB Using 3. Complex **3** (115 mg, 0.167 mmol) was added to a 50 mL round-bottom flask and dissolved in THF (ca. 25 mL). While the solution was stirring, AB (105 mg, 3.40 mmol) was added, and the reaction was allowed to proceed for ca. 1 h. The resulting precipitate was collected on a glass frit, washed with THF, and dried to yield a grayish-white solid (89 mg, 91%) (see Supporting Information for IR spectrum).

Dehydrogenation of DMAB Using 3. Complex **3** (21 mg, 0.031 mmol) was added to a solution of 20 mg (0.34 mmol) dimethylamine−borane dissolved in 2 mL of 1,2-dimethoxyethane. The red solution slowly turned to black with some black precipitate. After 12 h at 20 °C a 1 mL aliquot was withdrawn from the vial and combined with 3 drops of C_6D_6 in a 5 mm NMR tube for ^{11}B NMR analysis.

Generation of 5. To a solution of 21 mg (0.1 mmol) of *N*,*N*′-diphenylethylenediamine in 1 mL of 1,2-dimethoxyethane was added 200 uL of a 1 M solution of borane−THF in THF. After 6 h at 20 °C, the colorless sample was transferred to a 5 mm NMR tube, and 3 drops of C_6D_6 were added for ^{11}B NMR analysis. Observed products were the diamine bis(borane) and **5** in a 4:1 ratio.

■ ASSOCIATED CONTENT

Ⓢ Supporting Information

Supplementary spectra, X-ray diffraction tables and CIF files for compounds **3** and **4**, and complete refs 34 and 53. This material is available free of charge via the Internet at http://pubs.acs.org.

AUTHOR INFORMATION

Corresponding Author

jgordon@lanl.gov

Present Address

[‖]QD Vision, Inc., Watertown, MA 02472

Notes

The authors declare no competing financial interest.

ACKNOWLEDGMENTS

This work was funded by the U.S. Department of Energy, Office of Energy Efficiency and Renewable Energy. J.C.G. thanks Michael Janicke for NMR spectrometer maintenance, and R.T.B. thanks the Canada Foundation for Innovation and the Ontario Research Fund for instrumentation within the CCRI and Glenn Facey for assistance with the NMR spectrometers. The authors also thank the reviewers for their insightful suggestions.

REFERENCES

(1) Schlapbach, L.; Zuettel, A. *Nature* **2001**, *414*, 353−358.
(2) Satyapal, S.; Petrovic, J.; Read, C.; Thomas, G.; Ordaz, G. *Catal. Today* **2007**, *120*, 246−256.
(3) Technical System Targets: On-Board Hydrogen Storage for Light-Duty Vehicles (http://www1.eere.energy.gov/hydrogenandfuelcells/storage/pdfs/targets_onboard_hydro_storage.pdf).
(4) Marder, T. B. *Angew. Chem., Int. Ed.* **2007**, *46*, 8116−8118.
(5) Stephens, F. H.; Pons, V.; Baker, R. T. *Dalton Trans.* **2007**, 2613−2626.
(6) Klerke, A.; Christensen, C. H.; Nørskov, J. K.; Vegge, T. *J. Mater. Chem.* **2008**, *18*, 2304−2310.
(7) Wang, P.; Kang, X.-D. *Dalton Trans.* **2008**, 5400−5413.
(8) Peng, B.; Chen, J. *Energy Environ. Sci.* **2008**, *1*, 479−483.
(9) Chen, P.; Zhu, M. *Mater. Today* **2008**, *11*, 36−43.
(10) Murray, L. J.; Dinca, M.; Long, J. R. *Chem. Soc. Rev.* **2009**, *38*, 1294−1314.
(11) Hamilton, C. W.; Baker, R. T.; Staubitz, A.; Manners, I. *Chem. Soc. Rev.* **2009**, *38*, 279−293.
(12) Eberle, U.; Felderhoff, M.; Schüth, F. *Angew. Chem., Int. Ed.* **2009**, *48*, 6608−6630.
(13) Smythe, N. C.; Gordon, J. C. *Eur. J. Inorg. Chem.* **2010**, 509−521.
(14) Staubitz, A; Robertson, A. P. M; Manners, I. *Chem. Rev.* **2010**, *110*, 4079−4124.
(15) Conley, B. L.; Williams, T. J. *Chem. Commun.* **2010**, *46*, 4815−4817.
(16) Conley, B. L.; Guess, D.; Williams, T. J. *J. Am. Chem. Soc.* **2011**, *133*, 14212−14215.
(17) Sutton, A. D.; Burrell, A. K.; Dixon, D. A.; Garner, E. B. III; Gordon, J. C.; Nakagawa, T.; Ott, K. C.; Robinson, J. P.; Vasiliu, M. *Science* **2011**, *331*, 1426−1429.
(18) Chen, X.; Zhao, J. C.; Shore, S. G. *J. Am. Chem. Soc.* **2010**, *132*, 10658−10659.
(19) Ewing, W. C.; Marchione, A.; Himmelberger, D. W.; Carroll, P. J.; Sneddon, L. G. *J. Am. Chem. Soc.* **2011**, *133*, 17093−17099.
(20) Staubitz, A.; Robertson, A. P. M; Sloan, M. E.; Manners, I. *Chem. Rev.* **2010**, *110*, 4023−4078.
(21) Staubitz, A.; Sloan, M. E.; Robertson, A. P. M; Friedrich, A.; Schneider, S.; Gates, P. J.; Schmedt auf der Günne, J.; Manners, I. *J. Am. Chem. Soc.* **2010**, *132*, 13332−13345.
(22) Dallanegra, R.; Robertson, A. P.; Chaplin, A. B.; Manners, I.; Weller, A. S. *Chem. Commun.* **2011**, *47*, 3763−3765.
(23) Denney, M. C.; Pons, V.; Hebden, T. J.; Heinekey, D. M.; Goldberg, K. I. *J. Am. Chem. Soc.* **2006**, *128*, 12048−12049.
(24) Blaquiere, N.; Diallo-Garcia, S.; Gorelsky, S. I.; Black, D. A.; Fagnou, K. *J. Am. Chem. Soc.* **2008**, *130*, 14034−14035.
(25) Käß, M.; Friedrich, A.; Drees, M.; Schneider, S. *Angew. Chem., Int. Ed.* **2009**, *48*, 905−907.
(26) Kim, S. K.; Han, W. S.; Kim, T. J.; Kim, T. Y.; Nam, S. W.; Mitoraj, M.; Piekoś, Ł.; Michalak, A.; Hwang, S. J.; Kang, S.-O. *J. Am. Chem. Soc.* **2010**, *132*, 9954−9955.
(27) Keaton, R. J.; Blacquiere, J. M.; Baker, R. T. *J. Am. Chem. Soc.* **2007**, *129*, 1844−1845.
(28) Wright, W. R. H.; Berkeley, E. R.; Alden, L. R.; Baker, R. T.; Sneddon, L. G. *Chemm. Commun.* **2011**, *47*, 3177−3179.
(29) Jaska, C. A.; Temple, K.; Lough, A. J.; Manners, I. *Chem. Commun.* **2001**, 962−963. Jaska, C. A.; Temple, K.; Lough, A. J.; Manners, I. *J. Am. Chem. Soc.* **2003**, *125*, 9424−9434. Jaska, C. A.; Manners, I. *J. Am. Chem. Soc.* **2004**, *126*, 9776−9785.
(30) See Supporting Information in ref 27.
(31) Vance, J. R.; Robertson, A. P. M; Lee, K.; Manners, I. *Chem.—Eur. J.* **2011**, *17*, 4099−4103.
(32) Pons, V.; Baker, R. T.; Szymczak, N. K.; Heldebrant, D. J.; Linehan, J. C.; Matus, M. H.; Grant, D. J.; Dixon, D. A. *Chem. Commun.* **2008**, 6597−6599.
(33) Shrestha, R. P.; Diyabalanage, H. V. K.; Semelsberger, T. A.; Ott, K. C.; Burrell, A. K. *Int. J. Hydrogen Energy* **2009**, *34*, 2616−2621.
(34) Ott, K. C.; et al. Chemical Hydrogen Storage Research at Los Alamos National Laboratory, DoE Hydrogen Annual Progress Report, 2007 (http://www.hydrogen.energy.gov/pdfs/progress07/iv_b_5g_ott.pdf).
(35) Nutt, W. R.; McKee, M. L. *Inorg. Chem.* **2007**, *46*, 7633−7645.
(36) Zimmerman, P. M.; Paul, A.; Zhang, Z.; Musgrave, C. *Bioinorg. Chem.* **2009**, *48*, 1069−1081.
(37) Shaw, W. J.; Linehan, J. C.; Szymczak, N. K.; Heldebrant, D. J.; Yonker, C.; Camaioni, D. M.; Baker, R. T.; Autrey, T. *Angew. Chem., Int. Ed.* **2008**, *47*, 7493−7496.
(38) Ikariya, T.; Blacker, J. *Acc. Chem. Res.* **2007**, *40*, 1300−1308.
(39) Noyori, R. *Angew. Chem., Int. Ed.* **2002**, *41*, 2008−2022.
(40) Noyori, R.; Hashiguchi, S. *Acc. Chem. Res.* **1997**, *30*, 97−102.
(41) Andersen, R. A.; Faegri, K. Jr.; Green, J. C.; Haaland, A; Lappert, M. F.; Leung, W. P.; Rypdal, K. *Inorg. Chem.* **1988**, *27*, 1782−1786.
(42) Lin, P.-H.; Smythe, N. C.; Gorelsky, S. I.; Maguire, S.; Henson, N. J.; Korobkov, I.; Scott, B. L.; Gordon, J. C.; Baker, R. T.; Murugesu, M. *J. Am. Chem. Soc.* **2011**, *133*, 15806−15809.
(43) Sues, P. E.; Lough, A. J.; Morris, R. H. *Organometallics* **2011**, *30*, 4418−4431.
(44) Mikhailine, A. A.; Morris, R. H. *Inorg. Chem.* **2010**, *49*, 11039−11044.
(45) Paraskevi, O. L.; Lough, A. J.; Morris, R. H. *Inorg. Chem.* **2010**, *49*, 10057−10066.
(46) Mikhailine, A.; Lough, A. J.; Morris, R. H. *J. Am. Chem. Soc.* **2009**, *131*, 1394−1395.
(47) Sui-Seng, C.; Freutel, F.; Lough, A. J.; Morris, R. H. *Angew. Chem., Int. Ed.* **2008**, *47*, 940−943.
(48) Li, Y.-Y.; Zhang, X.-Q.; Dong, Z.-R.; Shen, W.-Y.; Chen, G.; Gao, J.-X. *Org. Lett.* **2006**, *8*, 5565−5567.
(49) Dong, Z.-R.; Li, Y.-Y.; Chen, J.-S.; Li, B.-Z.; Xing, Y.; Gao, J.-X. *Org. Lett.* **2005**, *7*, 1043−1045.
(50) Friedrich, A.; Drees, M.; Schneider, S. *Chem.—Eur. J.* **2009**, *15*, 10339−10342.
(51) Recent results from Manners et al. also point to the possibility of a solvent effect as generation of aminoborane in THF leads to insoluble poly(aminoborane): Robertson, A. P. M; Leitao, E. M.; Manners, I. *J. Am. Chem. Soc.* **2011**, *133*, 19322−19325.
(52) Sewell, L. J.; Lloyd-Jones, G. C.; Weller, A. S. *J. Am. Chem. Soc.* **2012**, *134*, 3598−3610.
(53) Frisch, M. J.; et al. *Gaussian 09*, Revision B.01; Gaussian, Inc.: Wallingford, CT, 2009.
(54) Ernzerhof, M.; Perdew, J. P. *J. Chem. Phys.* **1998**, *109*, 3313−3320.
(55) Roy, L. E.; Hay, P. J.; Martin, R. L. *J. Chem. Theory Comput.* **2008**, *4*, 1029.

(56) Formation of phosphine−borane from PCy_3 and AB requires elevated temperatures (see Figures S2, S4, and S5), which implies that unbound phosphine is not sufficient for phosphine−borane formation.
(57) Rossin, A.; Caporali, M.; Gonsalvi, L.; Guerri, A.; Lledós, A.; Peruzzini, M.; Zanobini, F. *Eur. J. Inorg. Chem.* **2009**, 3055−3059.
(58) Douglas, T. M.; Chaplin, A. B.; Weller, A. S.; Yang, X.; Hall, M. B. *J. Am. Chem. Soc.* **2009**, *131*, 15440−15456.
(59) Alcaraz, G.; Sabo-Etienne, S. *Angew. Chem., Int. Ed.* **2010**, *49*, 7170−7179.
(60) Alcaraz, G.; Chaplin, A. B.; Stevens, C. J.; Clot, E.; Vendier, L.; Weller, A. S.; Sabo-Etienne, S. *Organometallics* **2010**, *29*, 5591−5595.
(61) Chaplin, A. B.; Weller, A. S. *Inorg. Chem.* **2010**, *49*, 1111−1121.
(62) Ledger, A. E. W.; Ellul, C. E.; Mahon, M. F.; Williams, J. M. J.; Whittlesey, M. K. *Chem.—Eur. J.* **2011**, *17*, 8704−8713.
(63) Stevens, C. J.; Dallanegra, R.; Chaplin, A. B.; Weller, A. S.; Macgregor, S. A.; Ward, B.; McKay, D.; Alcaraz, G.; Sabo-Etienne, S. *Chem.—Eur. J.* **2011**, *17*, 3011−3020.
(64) Johnson, H. C.; Robertson, A. P. M; Chaplin, A. B.; Sewell, L. J.; Thompson, A. L.; Haddow, M. F.; Manners, I.; Weller, A. S. *J. Am. Chem. Soc.* **2011**, *133*, 11076−11079.
(65) Forster, T. D.; Tuononen, H. M.; Parvez, M.; Roesler, R. *J. Am. Chem. Soc.* **2009**, *131*, 6689−6691.
(66) *APEX II*, 1.08; Bruker AXS, Inc., Madison, WI, 2004.
(67) *SAINT+*, 7.06; Bruker AXS, Inc., Madison, WI, 2003.
(68) Sheldrick, G. *SADABS*, 2.03; University of Göttingen, Germany, 2001.
(69) *SHELXTL*, 5.10; Bruker AXS, Inc., Madison, WI, 1997.
(70) Farrugia, L. J. *J. Appl. Crystallogr.* **1997**, *30*, 565.
(71) Gangjee, A.; Wang, Y.; Queener, S. F.; Kisliuk, R. L. *J. Heterocycl. Chem.* **2006**, *43*, 1523−1531.